

Field Effect Modulation of Outer-Sphere Electrochemistry at Back-Gated, Ultrathin ZnO Electrodes

Chang-Hyun Kim and C. Daniel Frisbie*

Department of Chemical Engineering and Materials Science, University of Minnesota, 421 Washington Avenue SE, Minneapolis, Minnesota 55455, United States

S Supporting Information

ABSTRACT: Here we report field-effect modulation of solution electrochemistry at 5 nm thick ZnO working electrodes prepared on SiO₂/degenerately doped Si gates. We find that ultrathin ZnO behaves like a 2D semiconductor, in which charge carriers electrostatically induced by the back gate lead to band edge shift at the front electrode/electrolyte interface. This, in turn, manipulates the charge transfer kinetics on the electrode at a given electrode potential. Experimental results and the proposed model indicate that band edge alignment can be effectively modulated by 0.1–0.4 eV depending on the density of states in the semiconductor and the capacitance of the gate/dielectric stack.

The electrochemistry of semiconductors is central to the development of photoelectrochemical conversion systems^{1–5} and to understanding the geophotochemistry of light-absorbing minerals in water,⁶ for example. The recent advent of ultrathin two-dimensional (2D) semiconductor materials prepared either by exfoliation^{7,8} or thin film growth methods^{9,10} opens up new opportunities to examine the role of dimensionality in semiconductor electrochemistry.^{11–19} A particularly intriguing possibility explored here is to exploit the transverse field effect²⁰ (central to silicon CMOS technology) to modulate the carrier density in the valence (VB) and conduction bands (CB) of a 2D semiconductor that simultaneously serves as the working electrode (WE) in an electrochemical cell. This can be accomplished by placing the (grounded) 2D material on a metal gate/dielectric stack, **Figure 1a**, where application of voltage on the gate shifts the VB and CB edges with respect to the Fermi-level; this phenomenon is the transverse field effect.

The potential significance of such a field effect modulated WE architecture is 2-fold: (1) because of the extreme thinness of the 2D material, the charge induced in the semiconductor by the back gate should in principle be accessible to an electrolyte solution on the opposite (front) face; (2) this charge is separate from, but in addition to, double-layer charge induced by the independently controlled WE potential with respect to the reference (RE). We posit that such a gate tunable semiconductor electrode may open opportunities to modulate (reduce) electrochemical overpotentials for both outer-^{21–23} and inner-sphere^{24,25} (electrocatalytic) redox reactions and thus may serve as a useful platform for electrochemical investigations. To our knowledge, the possibility of gate tunable, ultrathin semiconductor electrodes has not been demonstrated before. For

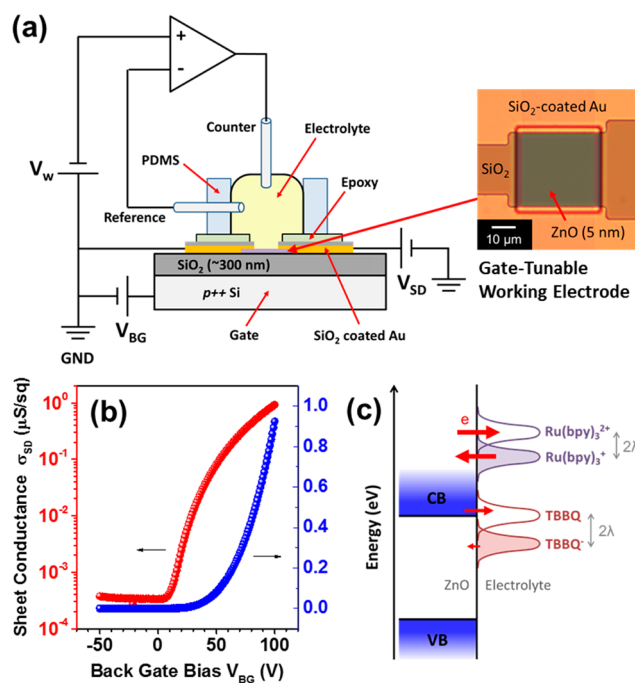


Figure 1. (a) Cross-sectional view of a back gated electrochemical cell with electrical/electrochemical configuration used in this study. The optical image on the right side shows a 5 nm thick ZnO electrode exposed through an epoxy window. (b) Sheet conductance (σ_{SD}) between two gold source and drain contacts versus back gate bias (V_{BG}) in N₂ atmosphere without electrolyte. The sheet conductance was obtained with $V_{SD} = 100$ mV. (c) Electron transfer (red arrows) at ZnO/electrolyte interface. Note that λ represents solvent reorganization energy, and TBBQ^{•-} and Ru(bpy)₃^{•+} have lower energy than TBBQ and Ru(bpy)₃²⁺, respectively, due to the solvent reorganization.

this initial demonstration, we focus on outer sphere redox chemistry at ultrathin ZnO electrodes, as described below.

ZnO electrodes on back gates were prepared following the procedure fully described in the [Supporting Information \(SI\)](#). Briefly, a ZnO layer was deposited on a SiO₂/p++ Si substrate (~300 nm thick oxide thermally grown on 525 μ m thick boron doped silicon wafer) by atomic layer deposition (ALD), followed by a series of annealing, photolithography, wet etching, and e-beam evaporation steps to make metal contacts and passivation layers that prevent electrochemical reaction from occurring on

Received: March 9, 2016

Published: June 1, 2016

the metal contacts. We prepared 5 and 50 nm thick ZnO electrodes, both of which show n-type characteristics upon reaching the threshold back gate bias, $V_{BG,th} \sim 10\text{--}20\text{ V}$ (Figures 1b and S8a); electrons induced at positive V_{BG} enhance sheet conductance of the ZnO layer between peripheral source and drain metal contacts while depletion of electrons at negative V_{BG} turns off the electronic conduction within the layer. To perform electrochemical tests while applying variable back gate biases, we configured the setup as shown schematically in Figure 1a (see SI for detail). All electrochemical measurements were performed at room temperature in a N_2 -filled glovebox with a three-electrode configuration: thin ZnO ($30 \times 30\ \mu\text{m}^2$) as the WE, platinum wires as quasi-reference and counter electrode (100 and 500 μm in diameter, respectively), and the room temperature ionic liquid 1-butyl-3-methylimidazolium bis-(trifluoro-methylsulfonyl) imide ([BMI][TFSI]) as supporting electrolyte and solvent. WE potentials in redox-active electrolytes, if not specified, are reported vs $\text{Fc}^{0/+}$ (the redox potential of ferrocene/ferrocenium) by using the redox species in the electrolyte as an internal standard (see SI for detail).

We conducted cyclic voltammetry (CV) measurements on 5 nm thick back gated ZnO electrodes in 10 mM 2,3,5,6-tetrabromo-1,4-benzoquinone (TBBQ) or 10 mM tris(2,2'-bipyridine) ruthenium(II) hexafluorophosphate ($\text{Ru}(\text{bpy})_3(\text{PF}_6)_2$) dissolved in [BMI][TFSI] (Figure 2). For the case of TBBQ voltammetry, it is crucial to note that the formal potential E° lies below the CB edge ($\sim 0.7\text{ V}$ vs $\text{Fc}^{0/+}$) for ZnO^{26} (i.e., it lies in the band gap), as shown schematically in Figure 1c. The key result of our communication is thus shown in Figure 2a,

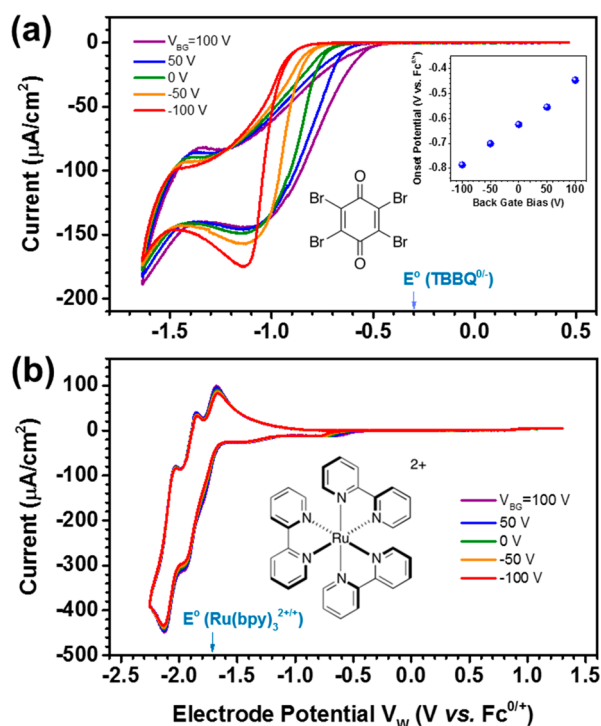


Figure 2. Cyclic voltammetry results of (a) TBBQ and (b) $\text{Ru}(\text{bpy})_3(\text{PF}_6)_2$ at a 5 nm thick ZnO electrode at different back gate biases (V_{BG}) from -100 to 100 V . Inset in (a) shows the onset potential (V_{ON}), where the CV current becomes greater than $1\ \mu\text{A}/\text{cm}^2$, for each V_{BG} . The arrows on x -axes in (a,b) indicate the formal potential (E°) of TBBQ $^{0/-}$ and $\text{Ru}(\text{bpy})_3^{2+/+}$, respectively. All CV experiments were conducted in 10 mM [BMI][TFSI] solutions at scan rate of $60\text{ mV}/\text{s}$.

which displays the CV for TBBQ at the 5 nm ZnO electrode as a function of back gate voltage (V_{BG} relative to a grounded contact on the ZnO, Figure 1a). At $V_{BG} = 0\text{ V}$ (the green curve in Figure 2a), the first reduction peak of TBBQ is observed at -1.05 V , which is $\sim 0.7\text{ V}$ more negative than E° (see SI for TBBQ CV at a gold electrode). A large overpotential is expected for TBBQ reduction at ZnO as E° lies in the band gap and a sufficient concentration of electrons in the CB must first accumulate, due to double layer charging, before reduction can commence. The important point evident in Figure 2a is that the onset of TBBQ reduction systematically shifts with V_{BG} . Positive V_{BG} shifts the CB edge down (more negative in electron energy), closer to E° , via the field effect. This results in a smaller overpotential for TBBQ reduction. Likewise, negative V_{BG} shifts the CB edge upward (more positive in energy) further from E° and increasing the overpotential. The shift is completely systematic and predictable based on a simple model described below. The absence of any significant reoxidation of TBBQ $^{\bullet-}$ in Figure 2a, at any gate voltage, is a consequence of the solvent reorganization energy 2λ (Figure 1c), which places the electronic manifold for TBBQ $^{\bullet-}$ even deeper in the band gap of ZnO. Thus, it is relatively easy, due to electronic state overlap, to reduce the TBBQ acceptor state once there is sufficient electron occupation of the higher lying ZnO CB, but the reverse process, reoxidation of TBBQ $^{\bullet-}$, is suppressed because of poor overlap between the TBBQ $^{\bullet-}$ electronic manifold and the CB.^{27,28}

The CV of $\text{Ru}(\text{bpy})_3^{2+}$ at an identical 5 nm thick ZnO electrode, shown in Figure 2b, serves as a control experiment because E° lies well above the CB edge for ZnO (Figure 1c). No overpotential is observed for multistep reduction of $\text{Ru}(\text{bpy})_3^{2+}$ because by the point at which the ZnO WE potential reaches E° , sufficient electron accumulation in the CB has occurred such that the ZnO surface in contact with the electrolyte is effectively metallic. Thus, reversible reduction and reoxidation of $\text{Ru}(\text{bpy})_3^{2+}$ can take place at the formal potential (-1.71 V) as is well-known in semiconductor electrochemistry.^{27,28} Importantly, this behavior is independent of V_{BG} as anticipated given that E° for this redox couple is well above the CB edge. Evidently, even very large negative V_{BG} biases are not sufficient to push the CB edge of ZnO above E° for $\text{Ru}(\text{bpy})_3^{2+}$. Altogether, the significant qualitative differences in the CVs for TBBQ and $\text{Ru}(\text{bpy})_3^{2+}$ support the concept that the transverse field effect can modulate the rates of judiciously chosen outer-sphere electron transfer processes at ultrathin semiconductor electrodes.

As noted already, critical to this concept is that the electrons induced by the back gate be accessible to the electrolyte solution on the front side of the ZnO. Thus, it is expected that thick ZnO WEs in the same back-gated configuration should not show gate modulated electrochemistry, i.e., when the thickness of the ZnO film is greater than the transverse electric field screening length, gate modulated electrochemistry at the ZnO/electrolyte interface should not occur. Indeed, we observed no gate modulation of TBBQ voltammetry at 50 nm thick ZnO electrodes (Figure S7a in SI), consistent with expectations. Further work is required to determine more precisely the critical thickness (between 5 and 50 nm) at which field effect modulation of the voltammetry can just be observed.

The electronic coupling between the front and back faces of the 5 nm ZnO layer can also be verified by examining the ZnO source-to-drain sheet conductance σ_{SD} as a function of its simultaneously controlled electrochemical potential V_W (i.e., “front gate” potential) and back-gate potential V_{BG} . Figure 3a displays σ_{SD} versus V_W at V_{BG} values ranging from -30 to 50 V . At

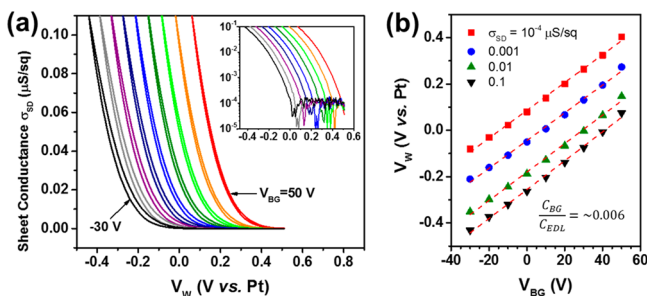


Figure 3. (a) Sheet conductance (σ_{SD}) of a 5 nm thick ZnO electrode in [BMI][TFSI] versus electrode potential (V_W) with back gate biases (V_{BG}) adjusted from -30 to 50 V with 10 V intervals. The sheet conductance was obtained with $V_{SD} = 10$ mV. The inset in (a) shows the same data on log scale. (b) V_W versus V_{BG} at designated σ_{SD} values.

any one V_{BG} value, σ_{SD} increases as V_W sweeps negative due to electric double layer charging of the ZnO/electrolyte interface. That is, negative V_W values result in electron accumulation in ZnO and turn the conductance of the film “ON”. There is a clear, systematic trend in the conductance onset with V_{BG} , namely, as V_{BG} becomes more positive the conductance onset shifts to more positive V_W . This is shown explicitly in Figure 3b, which plots V_W versus V_{BG} at specific values of σ_{SD} . The apparent linear relationship between V_W and V_{BG} can be explained by recognizing that the gate/dielectric/ZnO/electrolyte stack can be viewed as two series-coupled capacitors. The total charge Q_W on the thin ZnO WE is expressed to a first approximation as

$$Q_W = -C_{BG}V_{BG} + C_{EDL}V_W \quad (1)$$

where C_{BG} and C_{EDL} are the back gate and double layer capacitances, respectively. At fixed Q_W , corresponding to fixed σ_{SD} as in the Figure 3b plots, eq 1 predicts a linear relationship between V_W and V_{BG} with slope

$$\left(\frac{\partial V_W}{\partial V_{BG}}\right)_{\sigma_{SD}} = \frac{C_{BG}}{C_{EDL}} \quad (2)$$

Fits to the data in Figure 3b give $C_{BG}/C_{EDL} \approx 0.006$ consistent with the known capacitance of the 300 nm SiO_2 dielectric (~ 20 nF/cm²) and the estimated double layer capacitance (~ 10 $\mu\text{F}/\text{cm}^2$).

The data in Figure 3 demonstrate definitively that the front and back faces of the 5 nm ZnO layer are coupled; electron accumulations at the ZnO/dielectric and ZnO/electrolyte interfaces overlap, and thus, for a given sheet conductance, V_W and V_{BG} are strongly and predictably correlated. Importantly, identical sheet conductance measurements on 50 nm thick ZnO films revealed no correlation between V_W and V_{BG} (Figure S8b in SI), again indicating that for thicker ZnO the front and back interfaces are not electronically coupled. Altogether, the sheet conductance measurements support the conclusion from Figure 2a that the back-gate can modulate band-edge positions and redox chemistry at suitably thin ZnO working electrodes.

Schematic energy level diagrams shown in Figure 4 help to conceptualize the back-gating experiment. In creating these diagrams, we have assumed that the 5 nm thick ZnO is essentially a 2D semiconductor in which the energy band bending within the electrode can be ignored. Figure 4a depicts the initial state with $V_{BG} = 0$ V, where δ_0 represents the initial offset of the CB edge from E_F . Figure 4b corresponds to the application of $V_{BG} > 0$ V. In this case, the CB edge has shifted via the field effect closer to

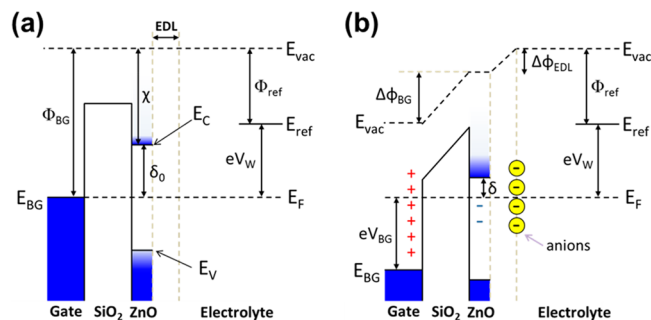


Figure 4. Energy diagrams of a back gated ultrathin ZnO electrode in electrolyte (a) before and (b) after a positive V_{BG} is applied to the back gate, while V_W is fixed. The symbols used in the diagram are as follows: CB edge (E_C) and VB edge (E_V) of ZnO, local vacuum level (E_{vac}); Fermi-levels of back gate (E_{BG}), ZnO (E_F), and RE (E_{ref}); work functions of back gate (Φ_{BG}) and RE (Φ_{ref}); electron affinity of ZnO (χ); vacuum level shifts in SiO_2 ($\Delta\phi_{BG}$) and EDL ($\Delta\phi_{EDL}$); CB edge offset (δ) from E_F in ZnO. Note that Φ_{BG} , Φ_{ref} and χ are assumed to be constant. Also note that the initial state ($V_{BG} = 0$ V) is depicted as the flat band condition for simplicity. More general energy diagrams can be found in Figure S10 in SI.

E_F ; the offset is now δ , and electron accumulation in the thin ZnO layer has occurred.

A detailed charge balance allows one to derive (see SI) the variation in the CB edge offset with respect to V_{BG} , namely:

$$\left(\frac{\partial \delta}{\partial V_{BG}}\right)_{V_W} = \frac{-e}{1 + \frac{C_{EDL}}{C_{BG}} + \frac{C_W(\delta)}{C_{BG}}} \quad (3)$$

where C_W is the quantum capacitance given by

$$C_W(\delta) = e \frac{dQ_W(\delta)}{d\delta} \quad (4)$$

Note that $C_W(\delta)$ essentially represents the density of states of the ZnO film in capacitance units, and thus, it has a strong dependence on δ (see Figure S11a in SI). From eqs 3 and 4, we can estimate band edge shift ($\Delta\delta$) achieved with application of V_{BG} at a given V_W . Assuming an ideal, trap state free ZnO film described with the free conduction electron model and $V_W = E_{TBBQ}^0$, $\Delta\delta$ can be ~ 0.4 eV for V_{BG} swinging from -100 to 100 V; for $V_W = E_{Ru(bpy)_3^+}^0$, the same V_{BG} range gives $\Delta\delta \approx 0.07$ eV (see SI). This result is qualitatively consistent with our observations. Since the reduction of TBBQ on ZnO occurs when the Fermi level is located near or well below the CB edge, where C_W is mostly negligible, TBBQ reduction kinetics can be effectively modulated by significantly shifting the band edge positions with V_{BG} . In contrast, redox reaction of $\text{Ru}(\text{bpy})_3^{2+}$ occurs at far more negative potential, where the ZnO undergoes a semiconductor-to-metal transition via EDL charging, and only small $\Delta\delta$ can be achieved due to the huge C_W (~ 45 $\mu\text{F}/\text{cm}^2$) in the potential range. Ultimately, the magnitude of $\Delta\delta$ will also be controlled by the choice of back gate dielectric material. Thin layers of high dielectric constant HfO_2 , for example, can increase C_{BG} 10-fold over the 300 nm SiO_2 layer employed here, allowing larger $\Delta\delta$ values to be obtained.

To summarize, we have demonstrated continuous, *in situ* modulation of electrochemical reaction kinetics on ultrathin semiconductors with voltage biases applied to a back gate. The onset potential of TBBQ reduction at a 5 nm thick ZnO electrode could be shifted by ~ 0.4 V with back gate biases. The sheet conductance measurements in electrolyte and the model

proposed in this work suggest that the observed gate-controlled redox reaction kinetics are essentially attributed to the shifts in band edge alignments at the electrode/electrolyte interface. Thus, the ability to control the band edge alignment independent of the working electrode potential should be generally useful for quantitative measurements of heterogeneous electron transfer rates at semiconductor/electrolyte interfaces.^{21,22} The application of the back gated electrode structure is not necessarily limited to the band alignment control demonstrated here but may also be employed to modulate surface chemisorption or degree of band bending for thicker films, for example. We believe that fundamental understanding of gate-controlled electrochemical phenomena will provide a new research platform and an optimization tool for various semiconductor-based electrochemical systems.

■ ASSOCIATED CONTENT

● Supporting Information

The Supporting Information is available free of charge on the ACS Publications website at DOI: [10.1021/jacs.6b02547](https://doi.org/10.1021/jacs.6b02547).

Materials, electrode fabrication procedure, electrical connections to the instruments, redox electrochemistry of TBBQ and Ru(bpy)₃(PF₆)₂ on gold and 50 nm thick ZnO electrode, sheet conductance of 50 nm thick ZnO electrode in N₂ and in [BMI][TFSI], determination of C_{BG} and C_{EDL} on gold electrodes, physical model for gate-tunable ZnO electrodes, and in-plane vs out-of-plane polarization during TBBQ redox cycle (PDF)

■ AUTHOR INFORMATION

Corresponding Author

*frisbie@umn.edu

Notes

The authors declare no competing financial interest.

■ ACKNOWLEDGMENTS

The authors thank Prof. Hong Chul Moon for providing the [BMI][TFSI], Dr. Seung Wook Shin and Dr. Donghoon Song for valuable discussions. C.K. acknowledges support of this project through Doctoral Dissertation Fellowship at the University of Minnesota. C.D.F. acknowledges additional support by NSF under Award No. ECCS-1407473. Parts of this work were carried out in the College of Science and Engineering Characterization Facility, University of Minnesota, which has received capital equipment funding from the NSF through the UMN MRSEC program under Award Number DMR-1420013, and in the Minnesota Nano Center, which receives partial support from NSF through the NNIN program.

■ REFERENCES

- (1) Wrighton, M. S. *Acc. Chem. Res.* **1979**, *12*, 303.
- (2) Bard, A. J. *Science* **1980**, *207*, 139.
- (3) Walter, M. G.; Warren, E. L.; McKone, J. R.; Boettcher, S. W.; Mi, Q.; Santori, E. A.; Lewis, N. S. *Chem. Rev.* **2010**, *110*, 6446.
- (4) Hagfeldt, A.; Boschloo, G.; Sun, L.; Kloo, L.; Pettersson, H. *Chem. Rev.* **2010**, *110*, 6595.
- (5) Tu, W.; Zhou, Y.; Zou, Z. *Adv. Mater.* **2014**, *26*, 4607.
- (6) Eggleston, C. M.; Stern, J. R.; Strellis, T. M.; Parkinson, B. A. *Am. Mineral.* **2012**, *97*, 1804.
- (7) Novoselov, K. S.; Geim, A. K.; Morozov, S. V.; Jiang, D.; Zhang, Y.; Dubonos, S. V.; Grigorieva, I. V.; Firsov, A. A. *Science* **2004**, *306*, 666.

- (8) Novoselov, K. S.; Jiang, D.; Schedin, F.; Booth, T. J.; Khotkevich, V. V.; Morozov, S. V.; Geim, A. K. *Proc. Natl. Acad. Sci. U. S. A.* **2005**, *102*, 10451.
- (9) Lee, Y. H.; Zhang, X. Q.; Zhang, W.; Chang, M. T.; Lin, C. T.; Chang, K. D.; Yu, Y. C.; Wang, J. T. W.; Chang, C. S.; Li, L. J.; Lin, T. W. *Adv. Mater.* **2012**, *24*, 2320.
- (10) George, S. M. *Chem. Rev.* **2010**, *110*, 111.
- (11) Tan, C.; Rodríguez-López, J.; Parks, J. J.; Ritzert, N. L.; Ralph, D. C.; Abruña, H. D. *ACS Nano* **2012**, *6*, 3070.
- (12) Ambrosi, A.; Chua, C. K.; Bonanni, A.; Pumera, M. *Chem. Rev.* **2014**, *114*, 7150.
- (13) Eady, S. C.; Peczonczyk, S. L.; Maldonado, S.; Lehnert, N. *Chem. Commun.* **2014**, *50*, 8065.
- (14) Voiry, D.; Yang, J.; Chhowalla, M. *Adv. Mater.* **2016**, 5597.
- (15) Hou, Y.; Laursen, A. B.; Zhang, J.; Zhang, G.; Zhu, Y.; Wang, X.; Dahl, S.; Chorkendorff, I. *Angew. Chem., Int. Ed.* **2013**, *52*, 3621.
- (16) Li, Y.; Wang, H.; Xie, L.; Liang, Y.; Hong, G.; Dai, H. *J. Am. Chem. Soc.* **2011**, *133*, 7296.
- (17) Jaramillo, T. F.; Jorgensen, K. P.; Bonde, J.; Nielsen, J. H.; Horch, S.; Chorkendorff, I. *Science* **2007**, *317*, 100.
- (18) Eisenberg, D. *ChemElectroChem* **2015**, *2*, 1259.
- (19) Kim, C.; Frisbie, C. D. *J. Phys. Chem. C* **2014**, *118*, 21160.
- (20) Neamen, D. A. In *Semiconductor Physics and Devices: Basic Principles*; McGraw-Hill, 2012; pp 371–490.
- (21) Hamann, T. W.; Gstrein, F.; Brunchwitz, B. S.; Lewis, N. S. *J. Am. Chem. Soc.* **2005**, *127*, 7815.
- (22) Hamann, T. W.; Gstrein, F.; Brunchwitz, B. S.; Lewis, N. S. *J. Am. Chem. Soc.* **2005**, *127*, 13949.
- (23) Lewis, N. S. *J. Phys. Chem. B* **1998**, *102*, 4843.
- (24) Bard, A. J. *J. Am. Chem. Soc.* **2010**, *132*, 7559.
- (25) Simpson, B. H.; Rodríguez-López, J. *J. Am. Chem. Soc.* **2015**, *137*, 14865.
- (26) Kohl, P. A.; Bard, A. J. *J. Am. Chem. Soc.* **1977**, *99*, 7531.
- (27) Nozik, A. J.; Memming, R. *J. Phys. Chem.* **1996**, *100*, 13061.
- (28) Gerischer, H. In *Physical Chemistry: An Advanced Treatise*; Eyring, H., Henderson, D., Yost, W., Eds.; Academic: New York, 1970; Vol. 9A, pp 463–542.